Characterization of V-type asteroids orbiting in the middle and outer main belt

Alessandra Migliorini [ID],[1]★ M. C. De Sanctis,[1] T. A. Michtchenko,[2]★ D. Lazzaro [ID],[3] M. Barbieri,[4] D. Mesa,[5] M. Lazzarin[6] and F. La Forgia [ID][6]

[1]*Institute of Space Astrophysics and Planetology, IAPS-INAF, Rome, Italy*
[2]*IAG, Universidade de Sao Paulo, São Paulo, Brazil*
[3]*Observatório Nacional, COAA, Rio de Janeiro, Brazil*
[4]*Instituto de Astonomía y Ciencias planetarias de Atacama, Univesity of Atacama, Copiapo, Chile*
[5]*Observatory of Padova, INAF-OAPd, Padova, Italy*
[6]*Department of Physics and Astronomy "G. Galilei", University of Padova, Padova, Italy*

ABSTRACT

We present new spectral observations using ground-based telescopes of 23 putative V-type asteroids, selected according to colour surveys in the visible from the Moving Objects Catalogue of the Sloan Digital Sky Survey and near-infrared from the Moving Objects VISTA catalogue. 10 asteroids are orbiting in the middle main belt, while five in the outer part of the main asteroid belt. For the observed asteroids, we assign a taxonomical classification and confirm the basaltic nature for 16 of them. The high-quality spectra in the UV range, obtained with the X-Shooter spectrograph at ESO, allowed the identification of the Fe^{2+} forbidden transition of pyroxene for 10 asteroids. This band is centred at 506.5 nm, and it is diagnostic of the Ca-content in the pyroxene form. We determined a low Fe-content composition for asteroids (2452) Lyot, (5758) Brunini, (7675) Gorizia, (9197) Endo, (22308) 1990 UO4, (36118) 1999 RE135, (66905) 1999 VC160, and (189597) 2000 WG119, and a composition more rich in Fe for asteroids (75661) 2000 AB79 and (93620) 2000 UQ70. We also present a dynamical investigation of V-type asteroids in the middle and outer main belt. The principal finding of these simulations is that the middle and outer V-types are more likely to be associated with some families, which were considered as possibly originated from the break up of a partially or totally differentiated parent body by diverse studies. This reinforces the hypothesis that the identified V-type in the region were not originated from (4) Vesta and that the number of differentiated objects in the middle and outer main belt must have been much larger than previously assumed.

Key words: techniques: spectroscopic telescopes – minor planets, asteroids: individual: Vesta.

1 INTRODUCTION

Basaltic material is reckoned as the result of an extensive geochemical differentiation resulting in a body with a dense metallic core, a mantle of lighter olivine-rich material, and an even lighter basaltic surface. This process should occur only on large-sized objects able to melt chondritic material (Ruzicka, Snyder & Taylor 1997; Wilson & Keil 2012). Asteroid (4) Vesta is the only large-sized object to show these characteristics whose spectrum presents two deep absorption bands, at ≈ 0.9 μm (known as BI) and at ≈ 2 μm (BII), representative of basaltic material.

Vesta shows also a well distinctive band at about 506 nm, due to a spin-forbidden transition of Fe^{2+} in the pyroxene structure (Cochran & Vilas 1998; Vilas, Cochran & Jarvis 2000; Cochran et al. 2004), and highly diagnostic of the Calcium-content of the pyroxene. This weak band was identified at different phases, weaker in case of phase angles that corresponded to the high elevation observed with the *Hubble*

Space Telescope (Vilas et al. 2000). The reported mean line centre occurs at 506.54 ± 0.45 nm. It was also detected by the imaging spectrometer Visible and InfraRed (VIR) onboard the NASA/Dawn mission, ranging between 0.505 and 0.507 nm in different regions (Stephan et al. 2015). The same composition is also observed on basaltic achondrite meteorites, specifically the Howardites, Eucrites, and Diogenites, collectively known as the HED suite of meteorites, for which (4) Vesta is considered the parent body (Pieters et al. 2000; Drake 2001).

An increasingly large number of small asteroids with a basaltic surface composition have been discovered all around the main belt (Xu et al. 1995; Lazzaro et al. 2000; Burbine et al. 2001; Florczak, Lazzaro & Duffard 2002; Alvarez-Candal et al. 2006), posing the focus on their origin and possible relation to Vesta or other parent bodies in the main belt. Asteroids have been classified as V-type if showing a visible spectrum similar to that of (4) Vesta (Tholen et al. 1989; Bus et al. 2002) or putative V-type if presenting compatible photometric colours in the visible (Roig & Gil-Hutton 2006; Carvano et al. 2010) or near-infrared (NIR) (Licandro et al. 2017). Most of V-type asteroids have orbital elements similar to Vesta, and count members of the so-called dynamical family or non-Vesta

★ E-mail: alessandra.migliorini@inaf.it (AM); tatiana.michtchenko@iag.usp.br (TAM)

family members. These objects have unique and well-distinguishable properties in terms of photometric colours, albedo, and spectral features (Masiero et al. 2015). They all show the absorption bands due to pyroxene and share spectral similarities with (4) Vesta (Duffard et al. 2006; Moskovitz et al. 2010; De Sanctis et al. 2011b, a; Ieva et al. 2016; Migliorini et al. 2017); they are characterized by a high albedo of 0.363 ± 0.088, although some variations are also possible. However, although comparison of spectroscopic data of V-types located in the family and in the non-family regions tends to suggest that some mineralogical differences may exist, no solid conclusions have been derived so far (Duffard et al. 2006; Moskovitz et al. 2010; De Sanctis et al. 2011a; Migliorini et al. 2017). Moreover, Jasmim et al. (2013), while observing some putative V-type asteroids, found that those located in the inner belt have a basaltic composition, but different from the one observed in the intermediate belt. This raises the question whether the putative V-type asteroids observed all around the main belt, but outside the Vesta region, are indeed basaltic or what kind of basaltic object they are.

One peculiar exception is represented by (1459) Magnya, a basaltic asteroid located at 3.14 AU from the Sun, with no clear dynamical link with existing asteroid families, large asteroids in the same outer belt region, and (4) Vesta (Lazzaro et al. 2000). Although similar to the HEDs, Hardersen, Gaffey & Abell (2004) have derived for (1459) Magnya a distinct mineralogy than (4) Vesta and the other V-type.

Considering the increasingly large number of small V-type asteroids identified in the middle and outer main belt that are likely not related to (4) Vesta, the question that arises is, how did they originate? According to our current understanding, a small asteroid presenting a basaltic surface should be a crust fragment of a larger differentiated body that suffered a catastrophic break up. Extensive numerical simulations of the dynamical evolution of Vesta's ejected fragments over time-scales comparable to the family age (Nesvorný et al. 2008) have shown that a relatively large fraction of the original Vesta family members may have evolved outside the family borders. These simulations also pointed out the lack of dynamical routes to transport Vesta's fragments to the intermediate and outer main belt, as well as to the lower inclinations in the inner belt. For all these objects a different origin must be searched.

We focused on asteroids, identified as *putative* V-types from photometric surveys (Roig & Gil-Hutton 2006; Carvano et al. 2010; Licandro et al. 2017). A total of 17 asteroids were observed in the UV-VIS-NIR using X-Shooter at the Very Large Telescope (VLT) (Vernet et al. 2011). Six more asteroids were observed in VIS-NIR with the DOLORES and NICS instruments at the Telescopio Nazionale Galileo (TNG). Our data set includes 10 asteroids with a semimajor axis $2.5 < a < 2.82$ AU (referred to as the m*iddle* main belt), and five with $a > 2.82$ AU (*outer* main belt). Our analysis focuses on providing a taxonomic classification of the observed asteroids, and investigates the presence of the most intense Fe-bearing pyroxenes spin-forbidden absorption band in asteroids that can be identified as V-types. In addition, we performed a numerical simulation to provide a dynamical context for the observed asteroids and the confirmed V-type asteroids in the middle and outer main belt (MB), previously reported in the literature. In this paper, data are described in Section 2, spectral properties are presented in Section 3, dynamical simulations are provided in Section 4. Conclusions follow.

2 DATA SELECTION, OBSERVATIONS, AND REDUCTION

In this survey, 17 potential V-type asteroids, of which 12 located at heliocentric distances >2.5 AU, have been observed with the X-

Shooter facility at ESO, on 2017 October 13–14 in visitor mode. Moreover, other six non-Vesta family asteroids, three of which located in the middle-outer belt, were spectrally investigated with the Telescopio Nazionale Galileo, on 2017 November 12–13 and 2018 April 4, during different observing runs. Asteroids were selected from lists of *putative* V-type asteroids, compiled according to their colours in the visible (Roig & Gil-Hutton 2006; Carvano et al. 2010) or in the NIR (Licandro et al. 2017) spectral ranges. The list of the observed asteroids and observing circumstances is reported in Table 1. Proper elements of observed asteroids, including semimajor axis (in AU), eccentricity, inclination (in deg), absolute magnitude (H), albedo, and diameters are listed in Table A1. Diameters from the Wide-field Infrared Survey Explorer (WISE) survey are reported when available (Masiero et al. 2013; Mainzer et al. 2019), while they are estimated considering an albedo of 0.363 similar to that of (4) Vesta for all the other cases. The listed diameters are in the range 1.1 and 11.8 km.

2.1 ESO/X-Shooter

The X-Shooter instrument (Vernet et al. 2011) is mounted on the ESO VLT telescope located on Cerro Paranale, Chile. It includes three arms that cover 0.3–0.5 µm, 0.5–1 µm, and 1–2.5 µm spectral ranges in one single acquisition. Hence, the complete spectrum in the optical and near-infrared is observed simultaneously, with a great advantage of time saving. Moreover, the three parts that compose the full spectral range can be directly joined without problems due to sky variability during the night. The small superposition between one range and the subsequent one allows to correctly join the three parts. For the UVB arm, we used a 1-arcsec slit width, with a readout of 100 K in high gain mode, that allows a resolving power of 4290, while we used a 0.9-arcsec slit for the VIS and NIR arms with a resolving power of 7410 and 5410, respectively. The nodding mode in the ABBA configuration was also imposed. It is used to acquire spectra of the target located in different positions on the array, namely A and B, close in time so that the sky background does not change a lot from an A acquisition to the subsequent B one. This technique allows to better estimate the sky background and properly subtract it. The slit was oriented along the parallactic angle, to avoid wavelength-dependent slit losses due to differential refraction by the Earth's atmosphere. Solar analogue HD11131 was also observed several times during the night at different airmass with the same instrument setup, to correct for the atmospheric contribution.

The calibration process includes bias and flat-field corrections, and wavelength calibration, that was performed following the ESO pipeline.[1] After the calibration process, asteroids spectra were divided by the solar analogue one in the closest observing conditions to those of the asteroids. UVB and VIS ranges were then joined, by properly vertically shifting the two parts in order to let them superpose in the 520–560 nm band. Similarly, the VIS and NIR ranges were joined in the $0.87 - 1.03$ µm band. Final asteroid spectra were obtained by taking the average of the ratio between asteroids and the solar analogue spectra in the two closest conditions observed during the nights.

2.2 Telescopio Nazionale Galileo

Asteroids (2168) Swope, (3331) Kvistaberg, (8805) Petrpetrov, (20188) 1997 AC18, (55613) 2002 TY49, and (61985) 2000 RW30

---

[1] Available at https://www.eso.org/sci/software/pipelines/xshooter/

Table 1. List of observed asteroids. Asteroids observed using ESO/X-Shooter instrument are reported in the upper part of the table, while asteroids observed with TNG are listed in the second part of this table. The columns indicate: (1) Asteroid name and number, (2) observing date, (3) UT time at the start of observation, (4) total exposure time (in seconds), (5) wavelength range in micron, (6) visual magnitude at the observing date, (7) survey, (8) solar analogue.

Asteroid	Date	UT$_{Start}$	Exp time (s)	Wvl range (μm)	V mag	Survey	Solar analogue
(2452) Lyot	2017 October 15	03:11:44	1723	0.3–2.5	16.3	(1)	HD11131
(5758) Brunini	2017 October 14	08:24:44	2647	0.3–2.5	17.3	(1)	HD11131
(7675) Gorizia	2017 October 15	02:18:42	3170	0.3–2.5	18.2	(1)	HD11131
(9197) Endo	2017 October 14	00:32:05	3319	0.3–2.5	18.1	(1)	HD11131
(10800) 1992 OM8	2017 October 14	04:34:50	3200	0.3–2.5	17.7	(1)	HD11131
(17239) 2000 EH95	2017 October 13	23:30:18	3660	0.3–2.5	18.3	–	HD11131
(22308) 1990 UO4	2017 October 14	23:18:25	3440	0.3–2.5	18.4	(2)	HD11131
(36118) 1999 RE135	2017 October 14	02:37:51	3313	0.3–2.5	17.9	(2)	HD11131
(48797) 1997 TV12	2017 October 14	05:32:02	4583	0.3–2.5	18.7	(2)	HD11131
(66905) 1999 VC160	2017 October 15	01:09:03	3111	0.3–2.5	18.2	(3)	HD11131
(67299) 2000 GS95	2017 October 14	01:28:10	3385	0.3–2.5	17.9	(2)	HD11131
(73076) 2002 GN4	2017 October 14	07:00:10	5044	0.3–2.5	18.7	(1)	HD11131
(75661) 2000 AB79	2017 October 15	07:31:51	3060	0.3–2.5	18.0	(1)	HD11131
(85812) 1998 WR22	2017 October 15	05:12:31	3120	0.3–2.5	18.2	(2)	HD11131
(93580) 2000 UC48	2017 October 15	04:00:42	4303	0.3–2.5	19.0	(2)	HD11131
(93620) 2000 UQ70	2017 October 15	06:04:38	4391	0.3–2.5	18.8	(2)	HD11131
(189597) 2000 WG119	2017 October 14	03:34:26	2841	0.3–2.5	17.3	(2)	HD11131
(2168) Swope	2017 November 13	03:05:40	1920	0.8–2.5	16.8	–	Land93-101; Land98-978
(3331) Kvistaberg	2017 November 12	21:02:53	2700	0.3–0.9	17.3	(1,3)	Land115-271; Land112-1333
(8805) Petrpetrov	2017 November 13	01:53:21	2880	0.8–2.5	17.0	–	Land93-101; Land98-978
(20188) 1997 AC18	2018 April 4	20:49:15	3584	0.8–2.5	17.3	(1)	Land98-978
(55613) 2002 TY49	2017 November 12	23:21:53	3700	0.3–0.9	18.3	–	Land115-271; Land112-1333
(61985) 2000 RW30	2017 November 13	04:34:25	3840	0.8–2.5	18.5	(1)	Land93-101; Land98-978

References: (1) Licandro et al. (2017); (2) Carvano et al. (2010); (3) Roig & Gil-Hutton (2006).

were observed with the TNG telescope, during two different programs. For asteroids (3331) Kvistaberg and (55613) 2002 TY49, only the visible spectrum in the wavelength range 0.3–0.9 μm was obtained, by using DOLORES, equipped with the LR-B and LR-R grisms. The other four asteroids were observed in the NIR spectral range, using the NICS instrument with the Amici grism. The Amici grism covers the 0.8–2.5 μm spectral band in one single acquisition, at a resolving power of about 50. For both configurations, we used a 2-arcsec slit aperture. This was oriented along the parallactic angle, to minimize the atmospheric refraction in case of the Low Resolution Spectrograph (LRS), while it was oriented along the asteroid motion for NICS, to minimize the target loss.

Data observed at TNG were reduced with standard routines, detailed in previous papers (Licandro, Ghinassi & Testi 2002; Lazzarin et al. 2004; De Sanctis et al. 2011a, b; Migliorini et al. 2017) and summarized in the following. We used the MIDAS software that allows to apply general routines for data calibration. To obtain the visible spectra of asteroids (3331) Kvistaberg and (55613) 2002 TY49, data were corrected for bias and for the non-uniformity of the images. Then, we obtained a one-dimensional spectrum for the wavelength calibration procedure that is performed by using spectra of Ne and Ar calibration lamps. Atmospheric absorption was removed by dividing for the solar analogue stars, observed with an airmass as closest as possible to the asteroid one. In this case, two solar analogues were available, Land 112–1333 and Land 115–271. The final spectra LR-B and LR-R were obtained by averaging the spectra resulting from the division by the two solar analogues.

The NIR spectra calibration does not require the bias subtraction. After flat-field correction, background is estimated and subtracted from consecutive observations acquired in a ABBA scheme, as in the case of ESO/XShooter spectra. The ABBA sequence is repeated until the total exposure time required to have the desired signal-

to-noise ratio is achieved. All the spectra acquired in the A and B positions are aligned and finally summed to obtain one spectrum that is equivalent to one with the total exposure time and with the sky background completely removed. Then wavelength calibration is performed. Asteroid spectra were finally obtained through division by the solar analogue star spectra (Land 93–101, Land 98–978). Spectral properties obtained from the above data are presented in the following section.

3 DATA ANALYSIS

3.1 Spectral appearance

The obtained spectra are presented in Fig. 1, for asteroids located in the outer MB region, in Fig. 2 for those in the middle MB, and in Fig. 3 for all the others, in the inner MB. Template spectra of spectroscopic classes, taken from DeMeo et al. (2009) are superposed to those observed, to better identify the classification proposed in our survey. In some cases, the spectral ranges at $1.3 - 1.5$ μm and $1.8 - 2.0$ μm are masked because the atmospheric correction is not good, especially in the case of spectra acquired with the ESO/X-Shooter instrument. In addition, we observe a decrease beyond 2.2 μm in the spectra of (67299) 2000 GS95 and (93580) 2000 UC48 (Fig. 2) that might be due to a poor correction of the atmospheric band and hence is not reliable.

According to their spectra, most of the asteroids, including (2452) Lyot, (55613) 2002 TY49 (Fig. 1), (20188) 1997 AC18, (22308) 1990 UO4, (36118) 1999 RE135, (61985) 2000 RW30, (66905) 1999 VC160, (93620) 2000 UQ70, and (189597) 2000 WG119 (Fig. 2), indicate a basaltic composition, and can be classified as V-types, based on the DeMeo classification (DeMeo et al. 2009). Asteroid (48797) 1997 TV12 (Fig. 1) is
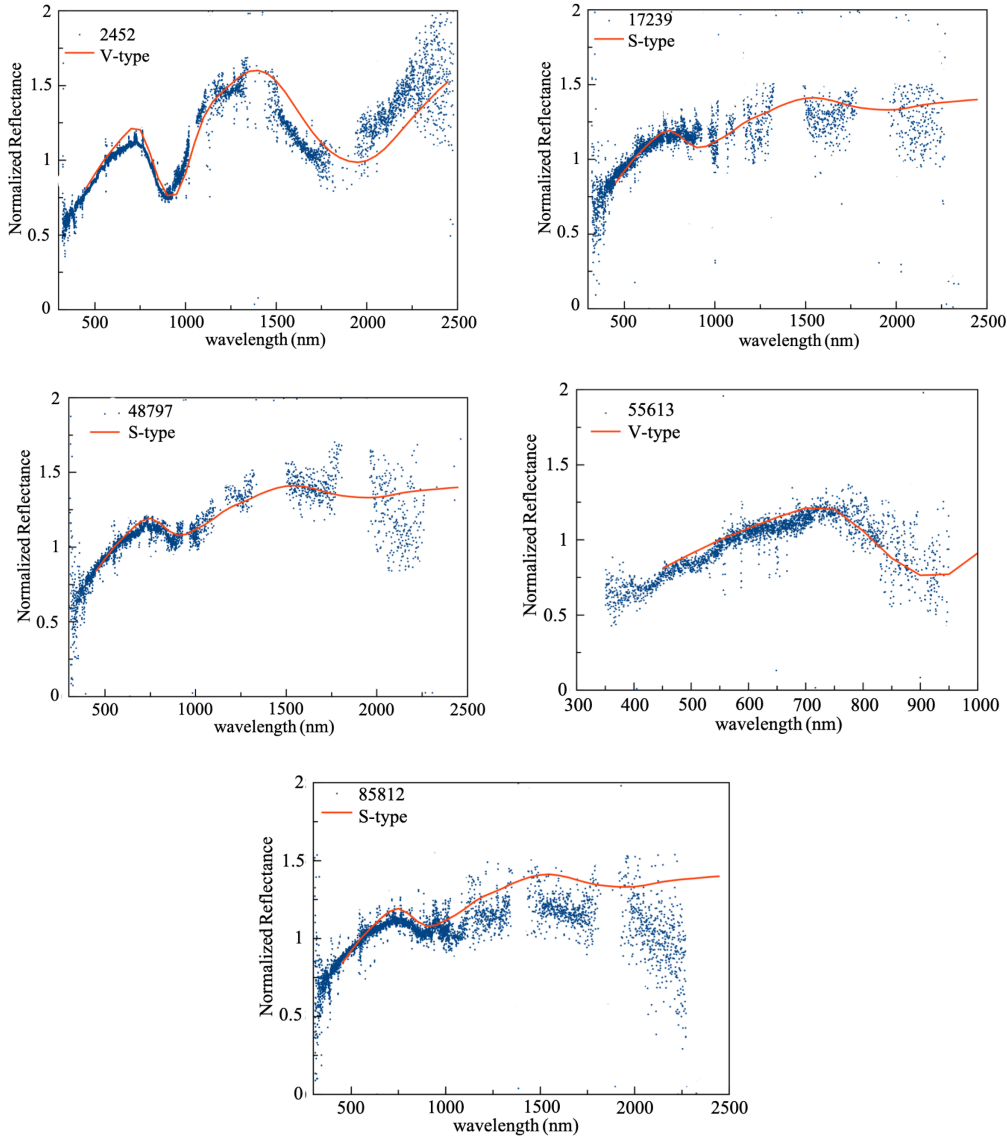
Figure 1. Spectra of asteroids with semimajor axis greater than 2.82 AU. Spectral regions where atmospheric bands are not well cleaned are removed from the spectra. Spectra obtained with X-shooter and TNG/DOLORES are normalized to 1 at 0.55 μm. Template spectra from DeMeo et al. (2009) are over-plotted to our data to clearly identify the proposed classification.

more compatible with the S_V class, asteroids (17239) 2000 EH95, (67299) 2000 GS95, (85812) 1998 WR22, and (93580) 2000 UC48 (Fig. 2) are compatible with S-type asteroids. The X-Shooter spectrum of (10800) 1992 OM8 shares similarities with Q- or S-types, and finally (73076) 2002 GN4 seems compatible with X-type objects. All observed asteroids located in the inner main belt are classified as V-type (Fig. 3). The only exception is asteroid (73076) 2002 GN4 that shows a featureless spectrum. If compared to the middle and outer main belt asteroids, the non-family basaltic objects located in the inner main belt region show similar band positions and depths, so that they seem to share a similar mineralogy. It can be noticed that asteroid (75661) 2000 AB79 has a very steep $1 - 1.5\,\mu m$ slope, indicative of a mineralogy different from the other V-types. However, variability in the basaltic composition among V-type asteroids in the inner and middle-outer main belt is suggested from previous surveys (Jasmim et al. 2013), as well as variations in the mineralogy among the family and non-family members (De Sanctis et al. 2011b).

In the Sloan Digital Sky Survey (SDSS; Stoughton et al. 2002), u'g'r'i'z' asteroid photometry is offered, and Hasselmann, Carvano & Lazzaro (2012) used data of the Moving Object Catalogue of this survey to classify the observed asteroids with different level of confidence. Asteroid (22308) 1990 UO4 (Fig. 1) indeed was potentially classified as a V_P-type with 96 per cent of probability (Hasselmann et al. 2012), in agreement with our finding. Similarly, asteroids (36118) 1999 RE135, (55613) 2002 TY49, (66905) 1999 VC160, (85812) 1998 WR22, (93620) 2000 UQ70 (Fig. 1), and (67299) 2000 GS95, and (93580) 2000 UC48 (Fig. 2) were classified as possible V-types in the same survey, with a lower probability, ranging between 11 and 37 per cent. However, while for asteroids (36118) 1999 RE135, (55613) 2002 TY49, (66905) 1999 VC160, and (93620) 2000 UQ70 spectra observed in this survey can confirm the classification as V-type, for (67299) 2000 GS95, (85812) 1998 WR22, (93580) 2000 UC48 another classification might be possible. Further investigation is required for these objects.
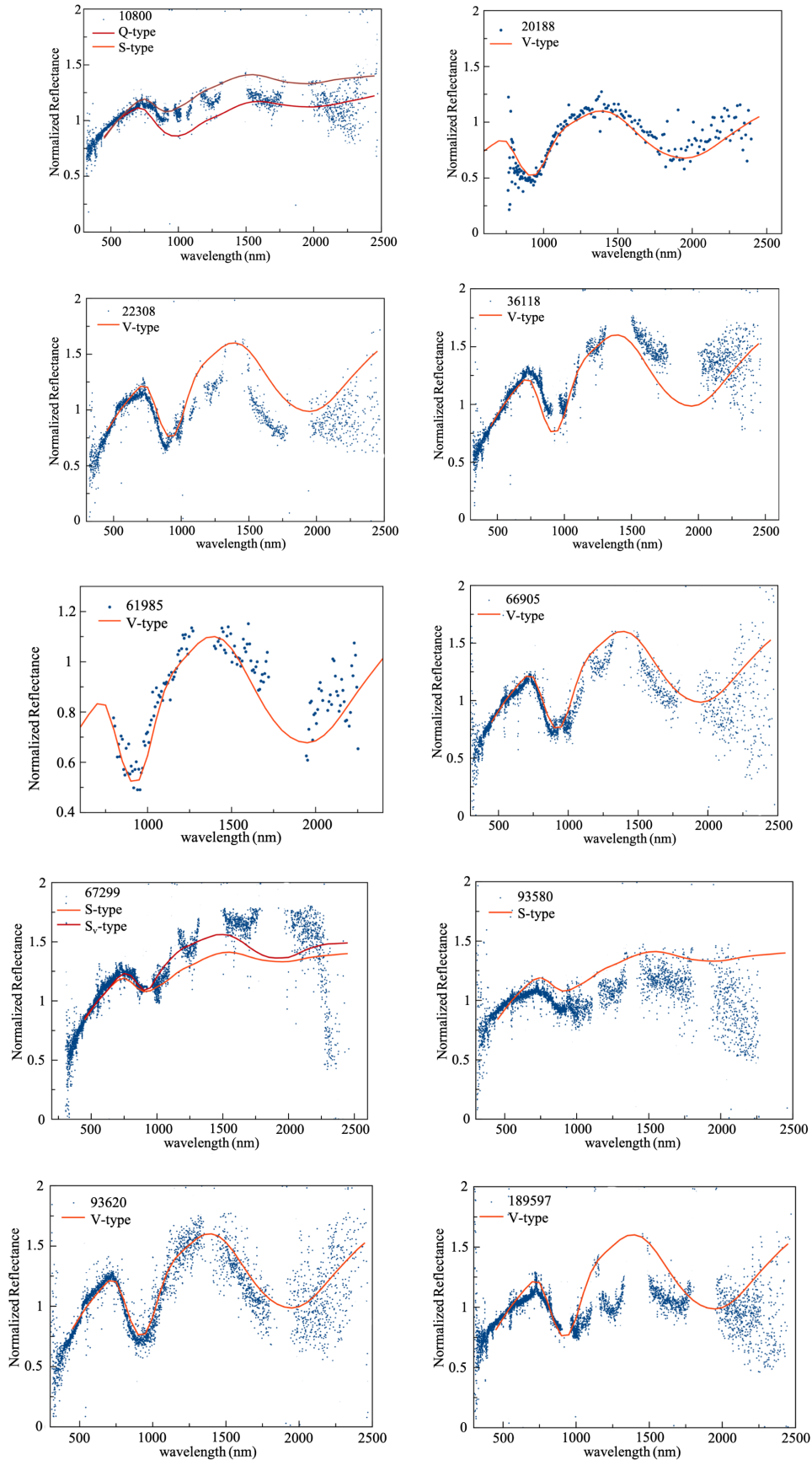
Figure 2. Spectra of the observed asteroids with semimajor axis semimajor axis 2.5 < *a* < 2.82 AU. Spectra obtained with X-shooter are normalized to 1 at 0.55 µm, while those acquired with TNG/NICS at 1.2 µm. Template spectra from DeMeo et al. (2009) are over-plotted to our data to clearly identify the proposed classification.
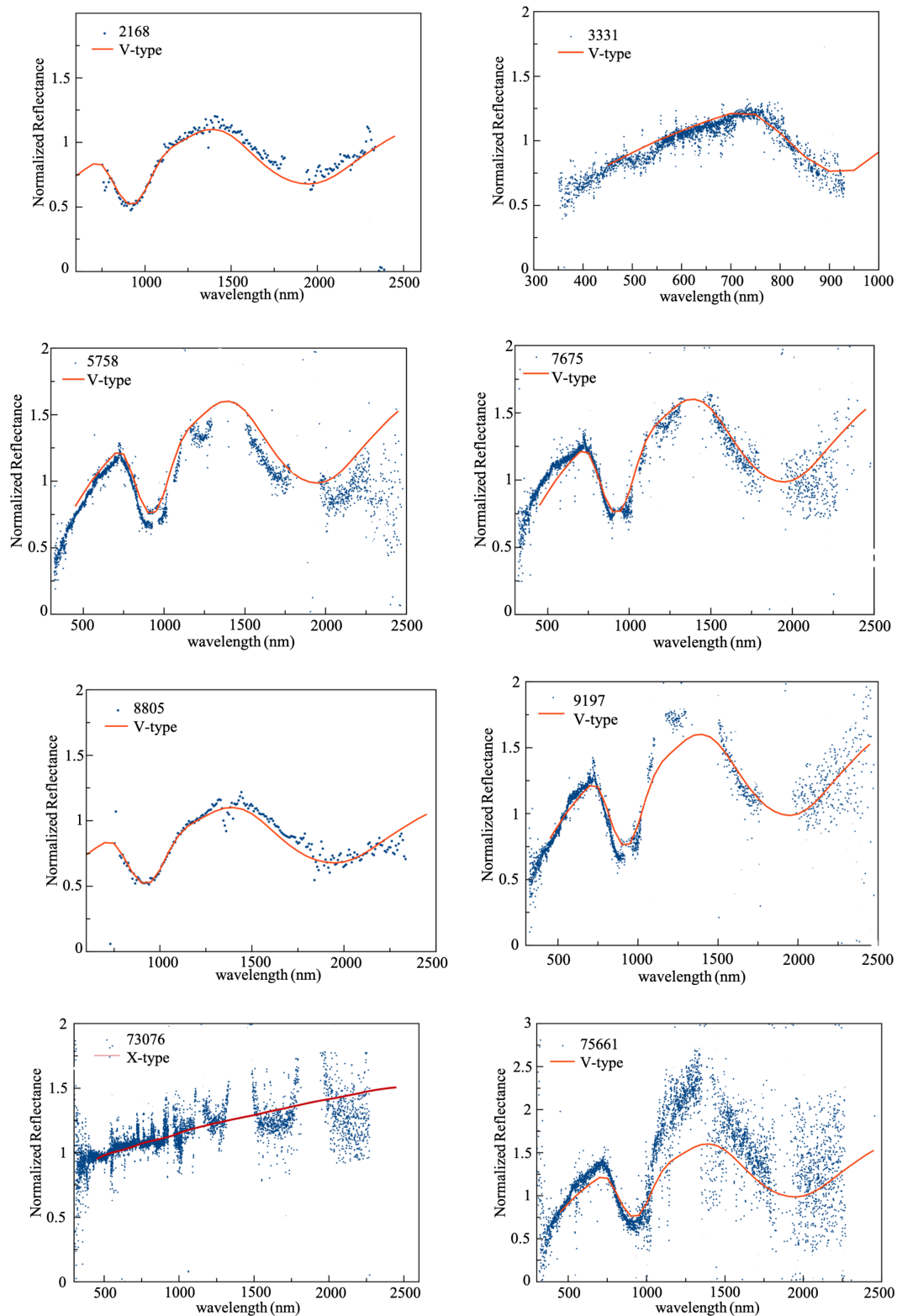
Figure 3. Spectra of the observed asteroids, located in the Vesta region. Spectra obtained with X-shooter and TNG/DOLORES are normalized to 1 at 0.55 μm, while those acquired with NICS at 1.2 μm. Template spectra from DeMeo et al. (2009) are over-plotted to our data to clearly identify the proposed classification.

Asteroid (48797) 1997 TV12 (Fig. 1) was classified as S_V, with a probability of 11 per cent; finally asteroid (189597) 2000 WG119 (Fig. 2) was assigned to the Q_v class (Hasselmann et al. 2012).

The WISE survey also offers a classification for asteroids, as well as the albedo and estimated diameters (Mainzer et al. 2019). According to this survey, (189597) 2000 WG119 is classified as Q_v while (48797) 1997 TV12 is linked to the 158 Koronis family and

classified as S_V-type. Asteroids (2168) Swope, (3331) Kvistaberg, (8805) Petrpetrov, (22308) 1990 UO4, (36118) 1999 RE135, (55613) 2002 TY49, (66905) 1999 VC160, and (93620) 2000 UQ70 are classified as V-types.

Asteroid (2452) Lyot (Fig. 1) was also observed in the visible with the *Isaac Newton Telescope* and near-infrared with the TNG, as shown in Medeiros et al. (2019). Although confirmed as a V-type, its composition is quite different from Vesta and (1459) Magnya, with a [Wo] content of 1.4–2.3 and a [Fs] of 21.3–23.6, more similar to a diogenitic composition. The spectrum of asteroid (36118) 1999 RE135 was reported also in Hardersen et al. (2018). For this asteroid, a basaltic composition is suggested, although with a slight enrichment in olivine or Ca-clinopyroxene content with respect to the average V-types and HED meteorites.

As shown in Carvano et al. (2015), asteroid classes V_P and Q_P overlap for the (z-i) colour index, with a slight superposition also with the O_P class. Hence, some asteroids might be confused with possible V-types, for which a confirmation with spectral insight in the VNIR is required. It must be said also that for some of these asteroids uncertainty in the classification remains due to the fact that the SDSS observations are flagged with the parameter 'BAD', which means that the derivation of at least one magnitude is uncertain above the third quartile (Hasselmann et al. 2015), and hence the assigned classification is not fully reliable. However, while for some asteroids observed in our survey the pyroxene bands at 1\$ and 2 μm are clearly visible and easily ascribed to basalt, for some others the bands are less pronounced and it is more difficult to understand their spectral classification. It is case of asteroids (10800) 1992 OM8 (Fig. 2), (17239) 2000 EH95 (Fig. 1), (73076) 2002 GN4 (Fig. 3), (85812) 1998 WR22 (Fig. 1), and (189597) 2000 WG119 (Fig. 2).

We finally checked the new classification based on the spectrophotometric data in the MOVIS-C catalogue (Mansour et al. 2020). In this classification, a composition fully compatible with diogenitic material is suggested for asteroid (2452) Lyot, in agreement with Medeiros et al. (2019) and our classification, while asteroid (20188) 1997 AC18 is confirmed as a V-type, in agreement with our spectra. For asteroids in the Vesta region (Fig. 3), the same survey suggests a basaltic composition similar to howardites in case of asteroids (5758) Brunini and (9197) Endo, and similar to Eucrite in case of asteroid (7675) Gorizia (Mansour et al. 2020) in agreement with our results.

It is worth noting that although photometric colours in the visible and NIR ranges might suggest a possible taxonomic classification, spectral investigations allow to a more reliable classification. In our analysis, only 15 of the 23 observed asteroids confirm the preliminary taxonomy classification based on NIR photometric colours from Licandro et al. (2017). This suggests that spectral investigation is crucial to ascertain the nature of observed asteroids and constraint their surface compositions, previously identified by photometric surveys.

Although some of the asteroids observed in this survey present a good signal-to-noise ratio spectrum that helps in constraining the taxonomic classification, not all spectra can be used to quantitatively investigate the surface composition of the basaltic asteroids identified within the survey. On the other hand, we found that the UV and VIS parts of ESO/X-Shooter spectrograph had the best contrast. In this respect, the UV part was inspected to investigate the presence of peculiar spin-forbidden absorption bands, typical of iron-bearing pyroxenes. In the following section, we describe the identification of one of these bands in the visible range.

3.2 The 506 nm band

Spectra acquired with ESO/X-Shooter have a higher spectral resolution than data obtained at TNG. This allowed the identification of one of the Fe-bearing pyroxenes spin-forbidden absorption bands in the visible spectral interval (Hazen et al. 1978; Klima, Pieters & Dyar 2007). The most prominent one, centred at 506 nm, is observed in most of the asteroids, obtained at ESO, which are also compatible with a V-type classification. The same feature was not identified in asteroids (3331) Kvistaberg and (55613) 2002 TY49, although the visible range is available, maybe due to the lower resolution of their spectra. This band is also superposed to other well-known atmospheric absorption bands; hence to exclude a possible contamination by the atmospheric contribution and better evidence the pyroxene band, spectra were divided by the one of asteroid (10800) 1992 OM8 that does not show any peculiar band in this spectral range. Final spectra in the UV region are shown in Fig. 4(a) with a vertical line that identifies the position at 506.5 nm. The applied procedure eliminates also other atmospheric bands, present in the same range, not properly corrected in the reduction process.

The 506 nm band is clearly visible in case of asteroids (2452) Lyot, (5758) Brunini, (7675) Gorizia, (9197) Endo, (22308) 1990 UO4, (75661) 2000 AB79, and (93620) 2000 UQ70, that are confirmed as V-types. The clear observation of this band, typical of pyroxenes, further strengthen the taxonomic classification. The same band is fainter in case of asteroids (36118) 1999 RE135 and (66905) 1999 VC160, although still present. It is interesting to note that, despite the poor quality VIS-NIR spectrum of asteroid (189597) 2000 WG119, the UV spectral range of its spectrum shows a faint decrease close to 506 nm, which indicates that the basaltic composition is valid for this asteroid as well. Due to these uncertainties, further investigation of asteroid (189597) 2000 WG119 would be desirable to better refine its taxonomic classification. The same technique was applied to all the asteroids observed with the ESO facility, regardless of their possible taxonomy, and shown in Fig. 4(b) for comparison. After the division by asteroid (10800) 1992 OM8, the spectra do not present any feature, but a slope, as in case of objects (48797) 1997 TV12, (67299) 2000 GS95, and (73076) 2002 GN4.

This band was observed in the spectrum of Vesta, centred at 506.54 ± 0.45 nm on average, with a different depth at different phase angles (Cochran & Vilas 1998; Vilas et al. 2000; Cochran et al. 2004). The authors also reported the detection of the 506 nm band in some vestoids, (2442) Corbett, (3869) Norton, (3155) Lee, and (2011) Veteraniya, as well as a possible weak band in the spectrum of (4038) Kristina and (2113) Ehrdni. These asteroids are located exterior to Vesta's orbit (Vilas et al. 2000), and have a proper orbital inclination angle similar to Vesta's or lower, while no correlation with eccentricity is reported (Cochran et al. 2004). It was also suggested that the presence of this forbidden transition was indicative of a young surface, but contrary to expectations, the same band was clearly observed on asteroids having a reddish spectrum (Hiroi et al. 2001). Variation in the band minima position of the 505–507 nm band was also reported for different regions on Vesta, observed by VIR on Dawn mission. The band was at longer wavelengths for regions dominant in eucrites and at shorter ones for pyroxenes similar to diogenites (Stephan et al. 2015). In our case, the visible and NIR portion of the observed spectra are contaminated by telluric lines that prevent the clear identification of band centre for BI and BII, as explained above. Hence any comparison with BI and BII cannot be applied in this case. However, all the spectra that present the 506.5 nm band have a reddish spectrum in the visible range, in agreement with Hiroi et al. (2001). Additional weaker bands at 425 and 550 nm can
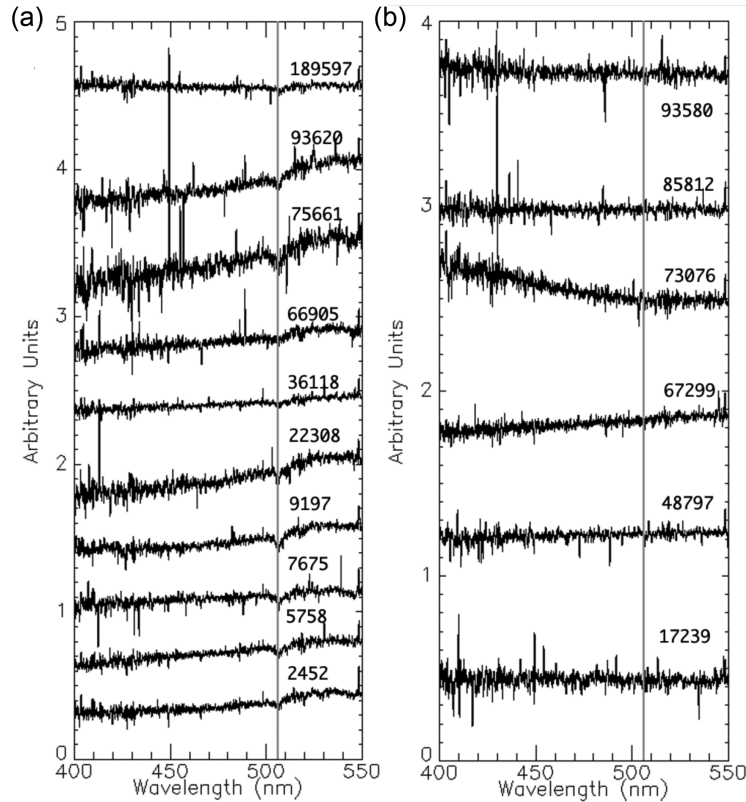
Figure 4. UV spectra of asteroids that (a) show the basaltic band at 506 nm, and (b) those that do not show the 506 nm band, observed with the UV channel of ESO/XShooter. Position at 506 nm is indicated by the vertical line for reference. Spectra are vertically shifted for a better visualization. Asteroid name is reported close to each spectrum.

also be observed in synthetic pyroxenes (Klima et al. 2007), although not clearly visible in our spectra, maybe because too faint. It should be noted also that the 550 nm band is close to the right edge of the UV detector of X-Shooter where also the signal performance degrades.

Laboratory measurements showed that pure diogenites have a band centre at 505.8 nm, at shorter wavelength than eucrites, where it is located at 507.6 nm (Hiroi et al. 2001). We noticed that the position of this band slightly moves to longer wavelengths with respect to the 506.5 nm position line in case of asteroids (75661) 2000 AB79 and (93620) 2000 UQ70, in our data set. This fact is compatible with an increasing iron content in the asteroid surfaces, according to laboratory investigation (Hiroi et al. 2001; Klima et al. 2007). Hence, for asteroids (2452) Lyot, (5758) Brunini, (7675) Gorizia, (9197) Endo, (22308) 1990 UO4, (36118) 1999 RE135, (66905) 1999 VC160, and (189597) 2000 WG119 we can suggest a basaltic composition with a low Fe-content, while for asteroids (75661) 2000 AB79, (93620) 2000 UQ70 a composition richer in eucrite is more likely. Finally, as demonstrated by a pulse-laser irradiation experiment, heavy space-weathering or a shock might erase the 506 nm feature in HED-like material (Hiroi et al. 2001). Hence further investigation in this spectral region would be helpful to shed light on possible variations in the 506 nm band observed in basaltic asteroids.

4 DYNAMICAL INVESTIGATIONS

The majority of the small basaltic asteroids in the middle and outer MB are not members of one of the currently identified dynamical families (e.g. Milani et al. 2014). On the other hand, they might have originated as part of dynamical families, but migrated to their

current locations due to the interplay of dissipative effects along with mean-motion and secular resonances. In order to further investigate this hypothesis, we analyse the distribution in the proper *a-e-i* space of 28 V-type objects from the middle and outer parts of the MB (see Table 2), including eight asteroids observed in this survey. We also perform several numerical simulations of their long-term evolution upon action of gravitational perturbations by the planets, from Mars to Neptune, and non-gravitational thermal Yarkovsky effects.

To simulate the Yarkovsky effects, we use SWIFT-RMVSY, the version of SWIFT modified by Brož (1999), to account for both the diurnal and seasonal versions of the Yarkovsky effect. We set the physical and thermal parameters as follows: $\rho_{bulk}=3500\,\mathrm{kg\,m^{-3}}$, $\rho_{surf}=1500\,\mathrm{kg\,m^{-3}}$, $K=2.65\,\mathrm{W\,m^{-3}\,K^{-1}}$ and $C=680\,\mathrm{J\,kg^{-1}\,K^{-1}}$, where ρ_{bulk}, ρ_{surf}, K, and C are bulk density, surface density, thermal conductivity, thermal capacity of the objects, respectively. The rotational period of an object is assumed to be inversely proportional to its radius (Farinella et al. 1998). The asteroid obliquity remains fixed at both $0°$ (prograde rotators) and $180°$ (retrograde rotators). In the former case, the diurnal Yarkovsky effect provokes the increase of the semimajor axis, while, in the latter case, the semimajor axis decreases. We do not consider reorientations of spin axis via collisions or The Yarkovsky–O'Keefe–Radzievskii–Paddack effect (YORP) (Čapek & Vokrouhlický 2004). The diameters and albedos of the objects were obtained from the JPL Small-Body Database Browser.[2] The results obtained for the observed objects are discussed in the following.

[2]https://ssd.jpl.nasa.gov/sbdb.cgi site

Table 2. List of selected asteroids for dynamical analysis. Asteroids of the middle MB are reported in the upper part of the table, while those of the outer in the second part. The columns indicate: (1) asteroid designation, (2) semimajor axis, (3) eccentricity, (4) inclination, (5) albedo, (6) references. Proper elements and family membership are taken from AstDys website. Albedo are obtained from the WISE survey (Mainzer et al. 2019), with the unique exception of (1459) Magnya, which is from Delbó et al. (2006).

Asteroid	a_p (AU)	e_p	i_p (deg)	Albedo	Family	References
(7459) Gilbertofranco	2.598	0.136	5.08	0.411 ± 0.026		(1)
(20188) 1997 AC18	2.593	0.057	7.70	0.229 ± 0.027		This paper
(21238) Panarea	2.541	0.133	10.55	0.373 ± 0.072		(2), (3), (4), (5), (6), (7)
(22308) 1990 UO4	2.773	0.074	12.29	0.157 ± 0.034		(6), (8), this paper
(23321) 2001 BY16	2.774	0.137	13.63	0.336 ± 0.082		(8)
(24014) 1999 RB118	2.561	0.141	13.06	0.244 ± 0.046	(15) Eunomia	(9)
(24264) 1999 XL143	2.768	0.147	9.05	0.364 ± 0.073	(93 Minerva	(8)
(36118) 1999 RE135	2.710	0.091	4.47	0.338 ± 0.077		(9), this paper
(40521) 1999 RL95	2.531	0.169	12.65	0.279 ± 0.032		(6)
(48448) 1990 WR2	2.539	0.171	7.58	0.277 ± 0.021		(8)
(61985) 2000 RW30	2.564	0.112	8.82	–		this paper
(63256) 2001 BY77	2.768	0.238	12.69	0.295 ± 0.111		(8)
(66905) 1999 VC160	2.746	0.122	13.26	–		this paper
(93620) 2000 UQ70	2.632	0.126	14.20	0.317 ± 0.135		this paper
(1459) Magnya	3.150	0.213	15.55	0.37 ± 0.06		(10), (11), (4), (5)
(2452) Lyot	3.158	0.157	11.72	0.380 ± 0.063		(1), this paper
(10537) 1991 RY16	2.850	0.103	6.34	0.313 ± 0.053		(4), (5), (6)
(10769) MinasGerais	3.072	0.068	9.35	0.161 ± 0.038	(221) Eos	(8)
(14447) Hosakakanai	3.015	0.254	8.64	0.093 ± 0.022		(8)
(14562) 1997 YQ19	3.121	0.173	16.62	0.156 ± 0.014		(8)
(27219) 1999 EL	3.113	0.198	16.88	0.223 ± 0.055	(1040) Klumpkea	(8)
(34698) 2001 OD22	3.180	0.069	22.72	0.373 ± 0.049		(9)
(41243) 1999 XG29	2.989	0.077	10.99	0.173 ± 0.030	(221) Eos	(8)
(47063) 1998 XX52	2.913	0.056	2.14	0.168 ± 0.040	(158) Koronis	(8)
(52002) 2001 UT30	2.997	0.084	10.30	0.205 ± 0.038	(221) Eos	(8)
(55613) 2002 TY49	2.914	0.025	8.03	–		this paper
(63085) 2000 WM135	3.138	0.085	11.88	–		(4)
(105041) 2000 KO41	3.040	0.158	10.64	–		(4), (5), (7)

References: (1) Medeiros et al. (2019); (2) Roig et al. (2008); (3) De Sanctis et al. (2011a); (4) Solontoi et al. (2012); (5) Ieva et al. (2016); (6) Leith et al. (2017); (7) Migliorini et al. (2018); (8) Ieva et al. (2018); (9) Hardersen et al. (2018); (10) Lazzaro et al. (2000); (11) Hardersen et al. (2004).

4.1 Objects from the outer belt

In Fig. 5 top panel, we plot, in the proper *a x i* space, the location of the selected spectroscopically confirmed V-type asteroids (full circles) in the outer region of the MB. Families identified in the AstDyS,[3] using the methodology presented in Milani et al. (2014), are also indicated. The colours, for both the objects and the families, represent the eccentricities according to ranges, as detailed in the chart. Therefore, objects and families with a same colour indicate that they share the same range of eccentricity. However, it must be kept in mind that the separation among the different eccentricity ranges is arbitrary and nearby colours, for example, green and red, might still represent a same region in the three-dimensional space of proper elements. In the figure, we also included some asteroids classified as M-type (crosses) and A-type (triangles) taken from the compilation by Neese (2010) to see their distribution and relation to families and V-type asteroids. It is worth noting that the break up of a differentiated, or partially differentiated, body is expected to produce fragments from the metallic nucleus (M-type) and/or mantle (A-type). However, a detailed analysis of the mineralogy of these objects is not straightforward and is outside the scope of the paper. The only point we would like to stress is that the presence of M-type and A-type nearby V-type asteroids is an

indication of the fragmentation of one or more larger differentiated bodies.

Fig. 5 (top panel) reveals an interesting feature: most of the V-types are in the vicinity, and in some case are even members, of a dynamical family. This is the case of objects (10769) MinasGerais, (41243) 1999 XG29, and (52002) 2001 UT30, members of the (221) Eos family, (27219) 1999 EL of the (1040) Klumpkea family, and (47063) 1998 XX52 of the (158) Koronis family (this membership is according to AstDyS). Moreover, asteroids (2452) Lyot and (105041) 2000 KO41 have semimajor axis and inclination in the range of the Eos family with just a little higher eccentricity (0.157–0.158, instead of 0.022–0.133), while asteroids (1459) Magnya and (14562) 1997 YQ19 lie very close to the Klumpkea family, having smaller inclinations.

The Eos family (the large green condensation in the centre in Fig. 5 top) was studied in detail by Mothé-Diniz et al. (2008). The spectra of 30 family members indicate that the bulk of the family is dominated by forsteritic olivine (Fa content of ~ 20 per cent), with orthopyroxene as a minor component. According to the authors, this composition is compatible with a body that was partially differentiated. Therefore, the presence of three spectroscopically confirmed V-type asteroids among the family tends to corroborate this result in further investigations. The dynamical evolution of these asteroids, as well as the three nearby, also makes it plausible their origin from the break up of a differentiated or partially differentiated parent body of the Eos family.

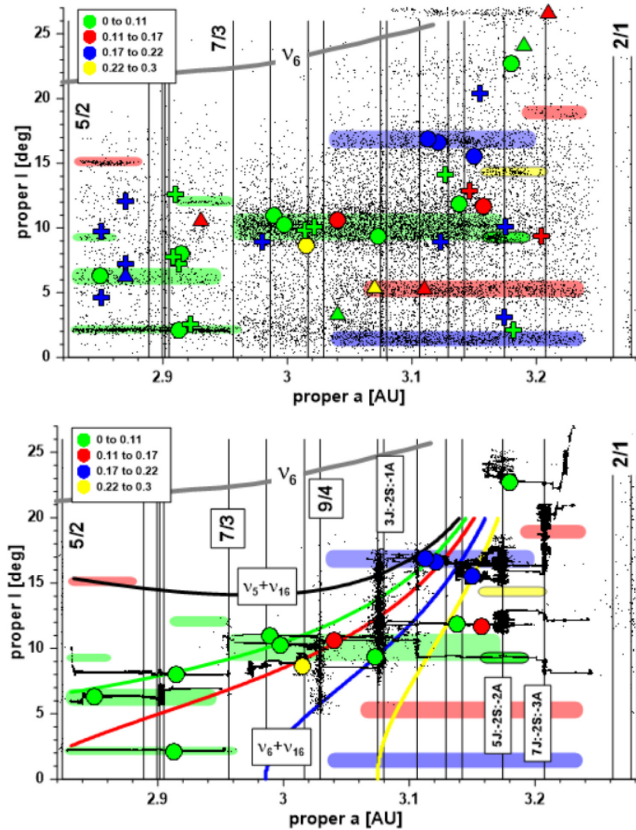[3]hamilton.dm.unipi.it/ astdys2/catalogs/allnum.pro

Figure 5. Top: *a x i* plane of the proper semimajor axis and inclination in the outer part of the MB. The distribution of the 14 V-type objects from Table 2 is shown by full circle. Some objects classified as M-type and A-type are shown by crosses and triangles, respectively. The main asteroidal families are shaped schematically by different colours that define the eccentricity ranges of the family members (see colour box). The colours of the symbols are chosen from the same ranges. The two- and three-body mean-motion resonances (MMRs) are shown by the vertical lines, while the linear ν_6 secular resonance (SR) is shown by the thick curve. The black dots are background objects. Bottom: Main dynamical features on *a x i* plane shown in the top panel. The diffusion paths of the V-type particles are shown by black points (see text for details). The location of the non-linear $\nu_5 + \nu_{16}$ SR is shown by thin black curve, while the $\nu_6 + \nu_{16}$ SR is shown by four colour curves, each one corresponding to the eccentricity range from the chart.

The Klumpkea family (blue concentration in the upper right of Fig. 5 top panel), of which asteroid (27219) 1999 EL is member, was previously identified as Tirela (Nesvorný et al. 2005). Its members present very peculiar spectra, mostly being taxonomically classified as L*d*, and some as S, S*a*, S*l* or A, as reported by Mothé-Diniz & Nesvorný (2008). The only object observed in the VNIR was (1400) Tirela which presented a clear band at ∼ 2μm, being thus more compatible with an L$_d$ classification. This spectrum does not have counterpart with known meteorites, but shows similarities with pigeonite. The position and depth of the 2μm band are in very good match as well in the region from $1.1 - 2.5$μm. In the visible part, however, the spectra of (1400) Tirela and of the pigeonite mineral are quite distinct. According to the authors, this difference might be attributed to the presence of some low-phases mineral on the asteroid surface. However, what it is interesting is that this mineral is the primary mafic mineral of the differentiated Eucrites and Howardite meteorites. The identification of a member of the Tirela/Klumpkea family with a basaltic composition is thus not to be considered as

fortuitous. It is also to be noted that two other V-type asteroids lie in the vicinity of this family: (1459) Magnya, the first basaltic asteroid discovered in the outer MB, and (14562) 1997 YQ19.

Finally, V-type asteroid (47063) 1998 XX52 is a member of the Koronis family, one of the largest families in the MB (green in the lower left side in Fig. 5 top panel). Several studies on this family (Cellino et al. 2002; Mothé-Diniz, Roig & Carvano 2005; Erasmus et al. 2020) indicate that most of its members can be classified as S-type or S-complex, but with a relatively large taxonomic diversity among the family. Although this classification does not *a priori* indicates a composition related to differentiation, it does not exclude it. It is important to mention that the mean albedo of this family is relatively high, 0.238 according to Masiero et al. (2013) [note that these authors identify the family as (208) Lacrimosa]. In this sense, we cannot consider asteroid (47063) 1998 XX52, with an albedo of 0.168 ± 0.040 (Mainzer et al. 2019), as an interloper.

As mentioned above, some of the V-type asteroids in the region are not members of a family but are located very near to one. Therefore, in order to investigate if these objects can indeed originate from the break up that formed some of above mentioned families, we decided to investigate the dynamical evolution of the selected V-type asteroids. Fig. 5 (bottom panel) shows the results of a numerical simulation of the long-term evolution of the V-type objects upon perturbations of five planets, from Mars to Neptune, accounting for Yarkovsky effects. The full circles show the actual positions of the V-type objects in the proper *a x i* space; the colours of the circles indicate the eccentricity range to which each object belongs (see the colour box). The contours of the asteroidal families in the region are shown schematically using the colours in accordance to the family's eccentricity range. In addition, Fig. 5 (bottom) shows the dynamical features of the outer part of the MB. The positions of the two- and three-body MMRs with the planets are shown by vertical lines. The continuous curves show the location of the strong non-linear SRs, $\nu_5 - \nu_{16}$ (black curve) and $\nu_6 + \nu_{16}$ (four branches of the resonance coloured according to the eccentricity range).

The diffusion paths of the particles are shown on the *a x i* plane of the proper semimajor axis and inclination by black dots in Fig. 5 (bottom panel). They extend toward larger *a*-values (outward migration), when the objects are assumed to be prograde rotators; contrarily, in the case of retrograde rotation, the diffusion occurs towards smaller *a* (inward migration). Both kind of rotators are considered for each V-type asteroid. The typical diffusion of the objects under the Yarkovsky effect is described in detail in Carruba et al. (2005), Carruba, Michtchenko & Lazzaro (2007). The objects are undergone mainly to slow inward/outward migration in the radial direction. When the particle reaches a MMR, it is frequently captured in the resonant regime of motion along the MMR's locus [vertical lines in Fig. 5 (bottom)], increasing/decreasing the orbital eccentricity/inclination. The time span of staying in the resonance mainly depends on the diffusion rate: slower the rate, longer is the time, and the changes in the proper eccentricity/inclination are more significant. If the eccentricity is high, the particle can be ejected from the MB; contrarily, it leaves the MMR and continues its slow drift in the radial direction (now with the different proper eccentricity/inclination), up to reach another MMR or SR. The similar behaviour is observed when the object is captured in a strong non-linear SR [continuous lines in Fig. 5 (bottom)], which provokes very strong excitation of the asteroidal eccentricity and/or inclination.

As shown in Michtchenko, Lazzaro & Carvano (2016), in the outer zone of the MB, the dominating dynamical mechanisms are two- and three-body MMRs. They are dense in this region and many of them are crossing the (221) Eos and (1040) Klumpkea families causing

escape of the family members. The SRs are weaker in the outer region; however, there are still several records of their interaction with the asteroidal families in the region, for instance, with the (158) Koronis family (Tsiganis, Varvoglis & Morbidelli 2003) and the (221) Eos family (Vokrouhlický et al. 2006). Regarding the advanced ages of the Eos, Koronis, and Klumpkea families, 1.4, 1.5, and 0.7 Gyr, respectively (according to AstDyS), the dynamical erosion could explain the presence of the V-type objects which are outside (but still close to) these families. The definitive escape of the particles from the outer zone occurs due to the 5/2, 7/3, 9/4, and 2/1 MMRs with Jupiter and some low-order three-body MMRs. This seems to be the case of the two V-type asteroids, (14447) Hosakakanai and (34698) 2001 OD22. The first one is a low-eccentricity/high-inclination object that is close to the 9/4 MMR and shows highly unstable motion according to AstDyS. The second one is a high-eccentricity/low-inclination object that is close to the first-order 5J:-2S:-2A MMR and also shows irregular behaviour. Our numerical simulation indicates relatively rapid ejection of both objects from the MB. It is worth stressing that, due to the unknown physical and thermal properties of the objects, numerical simulations allow us only a qualitative study of the asteroidal evolution upon the dissipative forces, and, consequently, non-precise results for the time-scale of their dynamical paths.

4.2 Objects from the middle belt

In Fig. 6 (top panel), we plot, in the proper $a \times i$ space, the location of the selected spectroscopically confirmed V-type asteroids (full circles) from the middle region of the MB, in the same manner as done in Fig. 5 (top panel), for the outer belt. Some of the high albedo families identified in the AstDyS are also indicated (Milani et al. 2014). In this case, the situation is complicated by both a much denser concentration of objects and a much complex dynamical environment. According to AstDyS, only two objects are members of a family: (24014) 1999 RB118 of the (15) Eunomia family and (24264) 1999 XL143 of (93) Minerva family. Moreover, three V-type asteroids, (40521) 1999 RL95, (66905) 1999 VC160, and (93620) 2000 UQ70, lie very nearby the Eunomia family in the proper element space. However, the remaining V-type asteroids in the middle MB do not belong to any family, having eccentricities distinct from those of the several families that seem to occupy the same region in the $a \times i$ proper space.

In Carruba et al. (2007), the Eunomia family was already proposed as possible origin of asteroid (21238) Panarea. Authors discussed the possibility that this asteroid formed during the break up that originated the family and then migrated via MMRs and SRs to its present location, outside the family. In that paper, it was already mentioned that asteroid (15) Eunomia was likely a completely or partially differentiated body, as shown in previous works (Reed, Gaffey & Lebofsky 1997; Nathues et al. 2005). The derived surface composition, rich in olivine, is consistent with a differentiated body that lost its basaltic crust during the formation of the family. Moreover, the spectroscopic analysis of several members of the Eunomia family indicated an S-type general taxonomic classification, with a somewhat large dispersion among the spectra (Lazzaro et al. 1999). A more complete analysis of the family, based on the observation of nearly a hundred of its members, showed that with high probability the original body was just partially and not completely differentiated considering that no V-type asteroids had been found (Nathues 2010). Since these have now been identified, and more than one, we can thus argue that the parent body of the Eunomia family was indeed completely differentiated.
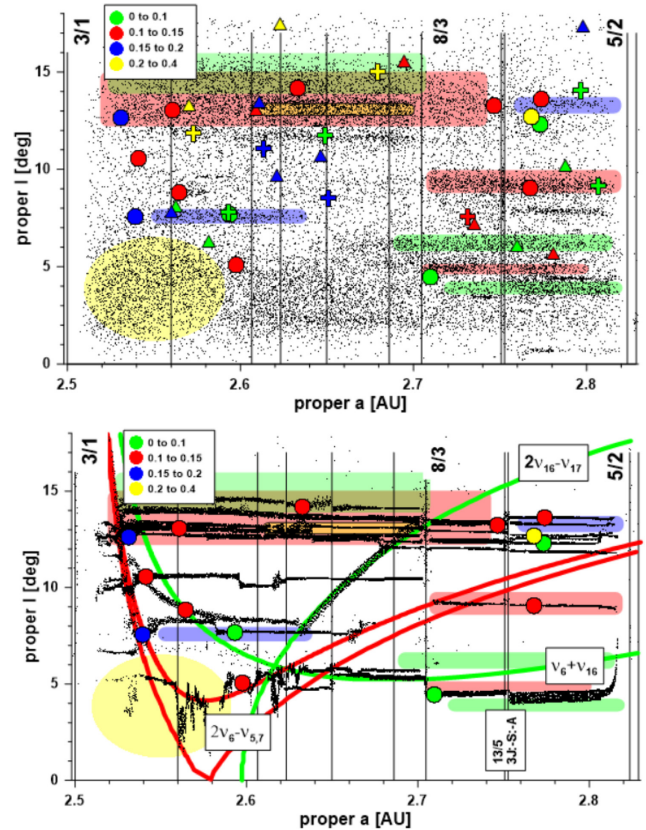

Figure 6. Top: Same as in Fig. 5 (top), except for the middle part of the MB. The main high-albedo families are identified by different colours corresponding to the eccentricity intervals from the chart. Bottom: Same as in Fig. 5 (bottom), except for the middle part of the MB. The main SRs are plotted by continuous curves; they are $2\nu_6 - \nu_5$ and $2\nu_6 - \nu_7$ (red lines), and $\nu_6 + \nu_{16}$ and $2\nu_{16} - \nu_{17}$ (green lines).

Regarding the V-type asteroid (24264) 1999 XL143, member of the Minerva family according to AstDyS, the situation is quite complex because the largest member of the family, asteroid (93) Minerva, has a C-type spectrum and a low albedo. This indicates that (24264) 1999 XL143 has a composition incompatible with the parent body which originated the Minerva family. However, we note that this family was identified as (1) Ceres or (1272) Gefion by several authors (Zappalá et al. 1995; Bus 1999; Mothé-Diniz et al. 2005; Nesvorný 2015) and, more recently, as (2595) Gudiachvili by Masiero et al. (2013). According to the latter, the mean albedo of the family is 0.265 and most of its members have a S-type taxonomic classification (as was the case of the Gefion family). The Gudiachvili family has, thus, a composition that can be compatible with the break up of a partially or completely differentiated body. This, indeed, is the conclusion derived by Blagen (2012) and more recently, by McGraw, Reddy & Sanchez (2018). These authors analysed the mineralogy of five asteroids members of the Gefion family (which are also identified as members of the Gudiachvili and Minerva families) concluding that they have properties similar to H chondrites, primitive, and basaltic asteroids. Moreover, they argue that the compositional diversity observed among the members of the Gefion family indicates the possibility of the parent body being partially differentiated. Therefore, we can conclude that the V-type composition of asteroid (24264) 1999 XL143 is not incompatible with the rest of the Gudiachvili/Gefion family.

Dynamical portrait of the middle zone of the MB is shown in Fig. 6 (bottom panel). The construction of the proper *a x i* plane is similar to that shown in Fig. 5 (bottom panel): the vertical lines indicate nominal locations of the main two- and three-body MMRs, while the continuous curves are used to indicate locations of the strong non-linear SRs. The asteroidal migration paths plotted by the black dots in Fig. 6 (bottom panel), clearly show that the large instabilities and consequent ejection of the objects are provoked by the 3/1, 5/2, and 8/3 MMRs with Jupiter. The three-body MMRs are weaker in the middle zone than the action of those in the outer zone. On the other hand, the low-order non-linear SRs are dense and strong in the middle belt, and, as shown in Michtchenko et al. (2016), their effects on the distribution of the real objects are noticeable in all eccentricities and at all inclinations. The mostly notable one is the boomerang-like structure, which is produced by the action of the two SRs, $2\nu_6 - \nu_5$ and $2\nu_6 - \nu_7$, whose locations at $e = 0.1$ are shown by two red curves in Fig. 6 (bottom). The overlap of these SRs provokes large instabilities in the asteroidal motion; (5) Astraea family, from the AstDyS catalogue, lies close to that region.

The behaviour of the particles is also influenced by the strong $\nu_6 + \nu_{16}$ and $2\nu_{16} - \nu_{17}$ SRs, whose location on the *a x i* plane is shown by two green curves of Fig. 6 (bottom); the effect of these SRs is significant for the low-eccentricity objects. We can observe capture and evolution of the particles along the loci of these resonances. This is the case of (61985) 2000 RW30, which migrates for a long time along the $2\nu_{16} - \nu_{17}$ SR, until to reach the 8/3 MMR with Jupiter and then to be ejected. The diffusion transport mechanisms acting in the middle zone of the MB seem to be more efficient in changing the proper elements of the objects, when compared to the processes in the outer belt. Considering that the Eunomia and Gefion families are 2 and 1 Gyr old, respectively, we can say that their members, which suffered the capture in the resonances during the long-lasting diffusion, would be currently unrecognizable as such. The six middle-belt V-type asteroids discussed here, located at a<2.6 AU, are actually involved in one of the SRs from this region.

5 CONCLUSIONS

We presented the spectra of 23 putative V-type asteroids, 10 of which located in the middle and 5 in the outer MB, obtained with ESO/X-Shooter and TNG in La Palma. The rest of the observed asteroids are non-family members located in the inner main belt region. For 16 of these newly observed asteroids, we confirm their basaltic composition, although a complete characterization was not possible due to strong atmospheric bands not well corrected. Our analysis of the UV channel of the X-Shooter spectra allowed the identification of one of the strongest Fe^{2+} forbidden transition of pyroxene, which is diagnostic of the iron and calcium content in the pyroxene form. This finding allowed suggesting a low Fe-content composition for asteroids (2452) Lyot, (5758) Brunini, (7675) Gorizia, (9197) Endo, (22308) 1990 UO4, (36118) 1999 RE135, (66905) 1999 VC160, and (189597) 2000 WG119, and a eucritic-rich composition for asteroids (75661) 2000 AB79 and (93620) 2000 UQ70.

The performed dynamical analysis showed that many of the V-type found in the middle and outer MB seem to be associated to some families that were considered as possibly originated from the break up of a partially or totally differentiated parent body by diverse studies (e.g. Mothé-Diniz & Nesvorný 2008; Nathues 2010). This result reinforces the hypothesis that the identified V-types in the region did not originated from (4) Vesta and that the number of differentiated objects in the middle and outer MB must have been much larger than previously assumed. These are now being identified due the

spectral analysis of the smaller bodies of the families. However, the complex dynamical evolution in these regions due to the interplay of several MMRs and SRs as well as the lack of more complete physical properties of the objects, in particular direction of rotation, does not allow defining the trajectory undergone by each object. It is worth stressing that, due to the unknown physical and thermal properties of the objects, numerical simulations allow us only a qualitative study of the asteroidal evolution upon the dissipative forces, and, consequently, non-precise results for the time-scale of their dynamical paths.

DATA AVAILABILITY

Data used in this paper include spectra acquired with ESO/X-Shooter and Telescopio Nazionale Galileo. Asteroid spectra are provided at the link http://dx.doi.org/10.20371/INAF/DS/2020_00004. Description of the data treatment can be found at the same link.

REFERENCES

Alvarez-Candal A., Duffard R., Lazzaro D., Mitchenko T., 2006, A&A, 459, 969
Blagen J. R., 2012, M. S. thesis, University South Dakota
Brož M., 1999, Diploma thesis, Charles Univ.
Burbine T. H., Buchanan P. C., Binzel R. P., Bus S. J., Hiroi T., Hinrichs J. L., Meibom A., McCoy T. J., 2001, Meteorit. Planet. Sci., 36, 761
Bus S. J., 1999, PhD thesis, Massachusetts Institute of Technology
Bus S. J., Binzel R. P., 2002, Icarus, 158, 146
Čapek D., Vokrouhlický D., 2004, Icarus, 172, 526
Carruba V., Michtchenko T. A., Lazzaro D., 2007, A&A, 473, 967
Carruba V., Michtchenko T. A., Roig F., Ferraz-Mello S., Nesvorný D., 2005, A&A, 441, 819
Carvano J. M., Hasselmann P. H., Lazzaro D., Mothé-Diniz T., 2010, A&A, 510, A43
Cellino A., Bus S. J., Doressoundiram A., Lazzaro D., 2002, in Bottke W. F., jr, Cellino A., Paolicchi P., Binzel R. P., eds, Asteroids III. The University of Arizona Press, Tucson, p. 182
Cochran A. L., Vilas F., 1998, Icarus, 134, 207
Cochran A. L., Vilas F., Jarvis K. J., Kelley M. S., 2004, Icarus, 167, 360

Delbó M. et al., 2006, Icarus, 181, 618

DeMeo F. E., Binzel R. P., Slivan S. M., Bus S. J., 2009, Icarus, 202, 160

De Sanctis M. C., Migliorini A., Luzia Jasmim F., Lazzaro D., Filacchione G., Marchi S., Ammannito E., Capria M. T., 2011b, A&A., 533, A77

De Sanctis M. C. Ammannito E., Migliorini A., Lazzaro D., Capria M. T., McFadden L., 2011a, MNRAS, 412, 2318

Drake M. J., 2001, Meteor. Planet. Sci., 36, 501

Duffard R., de León J., Licandro J., Lazzaro D., Serra-Ricart M., 2006, A&A, 456, 775–781

Erasumus N. et al., 2020, ApJS, 247, 13E

Farinella P., Vokrouhlický D., Hartmann W. K., 1998, Icarus, 132, 378

Florczak M., Lazzaro D., Duffard R., 2002, Icarus, 159, 178

Hardersen P. S., Gaffey M. J., Abell P. A., 2004, Icarus, 167, 170

Hardersen P. S., Reddy V., Cloutis E., Nowinski M., Dievendorf M., Genet R. M., Becker S., Roberts R., 2018, AJ, 156, 11

Hasselmann P. H., Carvano J. M., Lazzaro D., 2011, SDSS-based Asteroid Taxonomy V1.1. EAR.A.I0035-5-SDSSTAX-V1.1. NASA Planetary Data System, EAR–A-I0035-5-SDSSTAX-V1.0

Hasselmann P. H., Fulchignoni M., Carvano J. M., Lazzaro D., Barucci M. A., 2015, A&A, 577, A147

Hazen R. M. , Bell P. M., Mao H. K., 1978, Proc. Lunar Sci. Conf. 9th, 2919-2934, Vol. 3, Pergamon Press, New York

Hiroi T., Pieters C. M., Vilas F., Sasaki S., Hamabe Y., Kurahashi E., 2001, Earth Planets Space, 53, 1071

Ieva S., Dotto E., Lazzaro D., Fulvio D., Perna D., Mazzotta Epifani E., Medeiros H., Fulchignoni M., 2018, MNRAS, 479, 2607

Ieva S., Dotto E., Lazzaro D., Perna D., Fulvio D., Fulchignoni M., 2016, MNRAS, 455, 2871

Jasmim F. L., Lazzaro D., Carvano J. M. F., Mothé-Diniz T., Hasselmann P. H., 2013, A&A, 552, A85

Klima R. L., Pieters C. M., Dyar M. D., 2007, Meteor. Planet. Sci., 42, 235

Lazzarin M., Marchi S., Barucci M. A., Di Martino M., Barbieri C., 2004, Icarus, 169, 373

Lazzaro D. et al., 1999, Icarus, 142, 445

Lazzaro D. et al., 2000, Science, 288, 2033

Leith T. B., Moskovitz N. A., Mayne R. G., DeMeo F. E., Takir D., Burt B. J., Binzel R. P., Pefkou D., 2017, Icarus, 205, 61

Licandro J., Ghinassi F., Testi L., 2002, A&A, 388, L9

Licandro J., Popescu M., Morate D., de Léon J., 2017, A&A, 600, A126

Mainzer A., Bauer J., Cutrij R., Grav T., Kramer E., Masiero J., Sonnett S, Wright E., 2019, NEOWISE Diameters and Albedos V2.0. NASA Planetary Data System

Mansour J.-A., Popescu M., de León J., Licandro J., 2020, MNRAS, 491, 5966

Masiero J. R., DeMeo F. E., Kasuga T., Parker A. H., 2015, in Michel P., DeMeo F. E., Bottke W. F., eds, Asteroids IV, University of Arizona Press, Tucson, p. 323

Masiero J. R., Mainzer A. K., Bauer J. M., Grav T., Nugent C. R., Stevenson R., 2013, ApJ, 770, 7

McGraw A., Reddy V., Sanchez J. A., 2018, MNRAS, 476, 630

Medeiros H. et al., 2019, MNRAS, 488, 3866

Michtchenko T. A., Lazzaro D., Carvano J. M., 2016, A&A, 588, A11

Migliorini A., De Sanctis M. C., Lazzaro D., Ammannito E., 2017, MNRAS, 464, 1718

Migliorini A., De Sanctis M. C., Lazzaro D., Ammannito E., 2018, MNRAS, 475, 353

Milani A., Cellino A., Knežević Z., Novaković B., Spoto F., Paolicchi P., 2014, Icarus, 239, 46

Moskovitz N., Willman M., Burbine T., Binzel R., Bus S., 2010, Icarus, 208, 773

Mothé-Diniz T., Carvano J. M., Bus S. J., Duffard R., Burbine T. H., 2008, Icarus, 195, 277

Mothé-Diniz T., Nesvorný D., 2008, A&A, 492, 593

Mothé-Diniz T., Roig F., Carvano J. M., 2005, Icarus, 174, 54

Nathues A., 2010, Icarus, 208, 252

Nathues A., Mottola S., Kaasalainen M., Neukum G., 2005, Icarus, 175, 452

Neese C., ed., 2010, Asteroid Taxonomy V6.0. EAR-A-5-DDR-TAXONOMY-V6.0. NASA Planetary Data System

Nesvorný D., 2015, Nesvorny HCM Asteroid Families V3.0. EAR-A-VARGBDET-5-NESVORNYFAM-V3.0. NASA Planetary Data System

Nesvorný D., Brož M., Carruba V., 2015, in Michel P., DeMeo F. E., Bottke W. F., eds, Asteroids IV. University of Arizona Press, Tucson, p. 895

Nesvorný D., Jedicke R., Whiteley R. J., Ivezić Z., 2005, Icarus, 173, 132

Nesvorný D., Roig F., Gladman B., Lazzaro D., Carruba V., Mothé-Diniz T., 2008, Icarus, 193, 85

Pieters C. M. et al., 2000, Met. Planet. Sci., 35, 1101

Reed K. L., Gaffey M. J., Lebofsky L. A., 1997, Icarus, 125, 446

Roig F., Gil-Hutton R., 2006, Icarus, 183, 411

Roig F., Nesvorný D., Gil-Hutton R., Lazzaro D., 2008, Icarus, 194, 125

Ruzicka A., Snyder G. A., Taylor L. A., 1997, Meteor. Planet. Sci., 32, 825

Solontoi M. et al., 2012, Icarus, 218, 571

Stephan K. et al., 2015, Icarus, 259, 162

Stoughton C. et al., 2002, AJ, 123, 485

Tholen D. J., Barucci M. A., 1989, Asteroids II, Proceedings of the Conference. University of Arizona Press, Tucson, AZ, p. 298

Tsiganis K., Varvoglis H., Morbidelli A., 2003, Icarus, 166, 131

Vernet J. et al., 2011, A&A, 536, A105

Vilas F., Cochran A. L., Jarvis K. S., 2000, Icarus, 147, 119

Vokrouhlický D., Brož M., Morbidelli A., Bottke W. F., Nesvorný D., Lazzaro D., Rivkin A. S., 2006, Icarus, 182, 92

Wilson L., Keil K., 2012, Chem. Erde, 72, 289

Xu S., Binzel R. P., Burbine T. H., Bus S. J., 1995, Icarus, 115, 1

Zappalá V., Bendjoya P., Cellino A., Farinella P., Froeschlé C., 1995, Icarus, 116, 219

APPENDIX A: ORBITAL PARAMETERS OF OBSERVED ASTEROIDS

Table A1. List of observed asteroids. Asteroids observed using ESO/X-Shooter instrument are reported in the upper part of the table, while asteroids observed with TNG are listed in the second part of this table. The columns indicate: (1) Asteroid number, (2) semimajor axis, (3) eccentricity, (4) inclination, (5) absolute magnitude, (6) asteroid diameter (in km), (7) albedo, (8) location, (9) taxonomy, (10) Fe^{2+} band. Proper elements are taken from AstDys website, while absolute magnitude, diameters, and albedo are taken from the WISE survey (Mainzer et al. 2019).

Asteroid	a_p (AU)	e_p	i_p (deg)	H (mag)	Diam (km)	Albedo	Location	Taxonomy	Fe^{2+} band (Y/N)
(2452) Lyot	3.157	0.156	8.98	11.4	11.8	0.380	Outer	V	Y
(5758) Brunini	2.248	0.102	0.58	13.95	4.4	0.305	Inner	V	Y
(7675) Gorizia	2.414	0.1309	7.51	14.3	3.0	–	Inner	V	Y
(9197) Endo	2.163	0.043	2.46	14.8	3.2	0.211	Inner	V	Y
(10800) 1992 OM8	2.549	0.0924	5.30	14.4	3.3	0.343	Middle	Q-S	N
(17239) 2000 EH95	3.046	0.0462	2.65	12.7	10.4	0.113	Outer	S	N
(22308) 1990 UO4	2.773	0.1126	6.46	13.9	5.8	0.157	Middle	V	Y
(36118) 1999 RE135	2.709	0.0742	4.25	13.4	5.0	0.338	Middle	V	Y
(48797) 1997 TV12	2.939	0.0643	3.69	14.6	3.6	0.135	Outer	S_V	N
(66905) 1999 VC160	2.746	0.1459	8.39	14.9	2.3	–	Middle	V	Y
(67299) 2000 GS95	2.575	0.2691	15.60	14.6	2.9	0.230	Middle	S-complex	N
(73076) 2002 GN4	1.961	0.1019	21.18	15.3	1.9	–	Inner	X	N
(75661) 2000 AB79	2.373	0.1228	7.05	15.3	1.9	–	Inner	V	Y
(85812) 1998 WR22	2.844	0.1776	10.23	15.2	2.0	–	Outer	S	N
(93580) 2000 UC48	2.644	0.2865	16.65	16.5	1.1	–	Middle	S-complex	N
(93620) 2000 UQ70	2.633	0.1439	8.27	15.1	2.1	–	Middle	V	Y
(189597) 2000 WG119	2.658	0.1922	11.08	15.4	1.8	–	Middle	V	Y
(2168) Swope	2.453	0.1549	4.745	12.7	8.2	0.263	Inner	V	–
(3331) Kvistaberg	2.421	0.0868	3.566	13.4	4.6	–	Inner	V	–
(8805) Petrpetrov	2.341	0.154	2.773	14.4	2.9	–	Inner	V	–
(20188) 1997 AC18	2.593	0.1249	8.61	11.4	4.8	0.229	Middle	V	–
(55613) 2002 TY49	2.914	0.0238	8.01	14.5	2.8	–	Outer	V	–
(61985) 2000 RW30	2.564	0.0914	8.83	14.4	2.9	–	Middle	V	–

This paper has been typeset from a TEX/LATEX file prepared by the author.